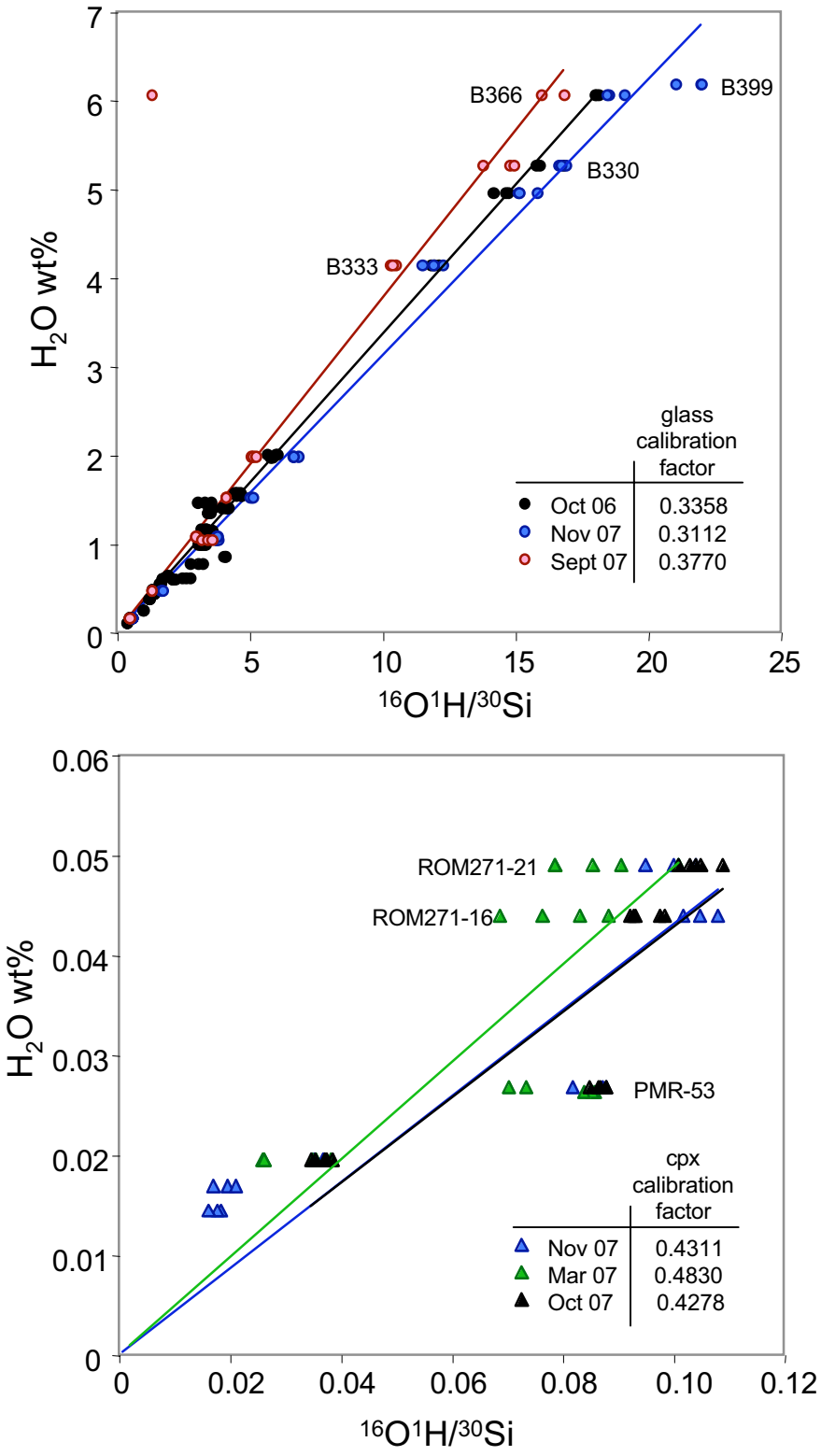

Data Repository

Figure DR1. Example calibration curves for SIMS analyses from different analytical sessions. For details see Hauri et al. (2002, 2006a,b). Calibration factors (e.g. line slopes) are listed adjacent to the run dates. Some glass standards > 2 wt% H_2O are listed for reference (see Hauri et al., 2006a and references therein for others), as are some cpx analyzed.

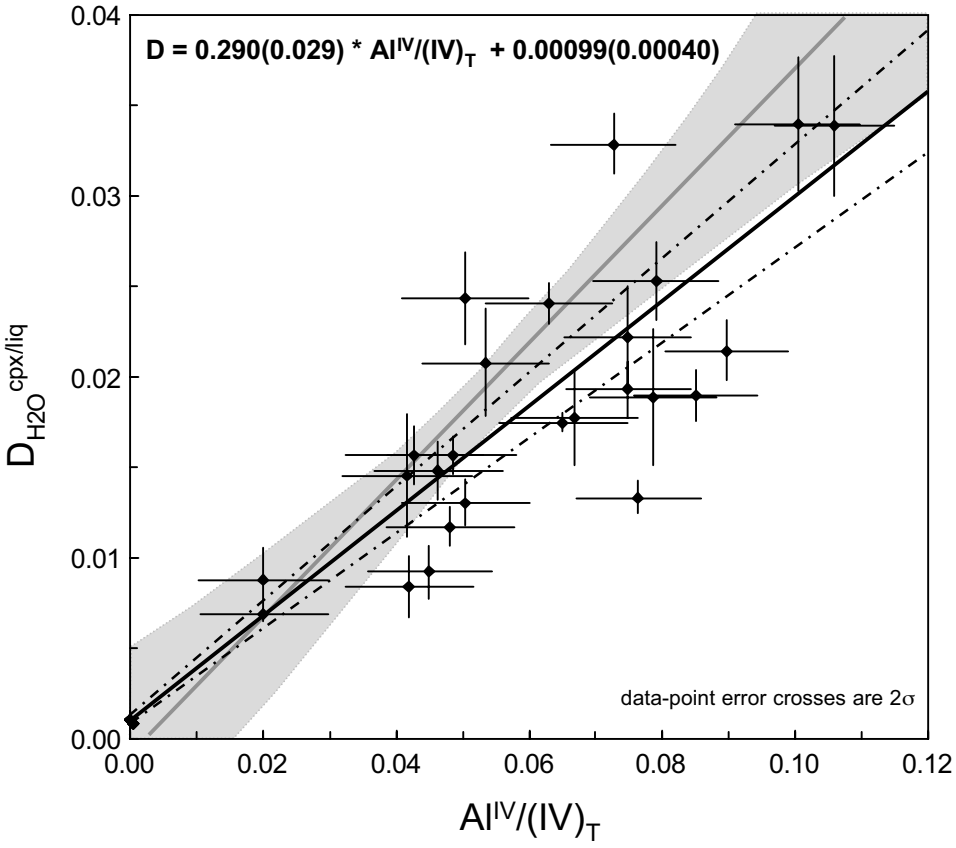

Data Repository

Figure DR2. Correlation of water partitioning between pyroxene and melt, and the proportion of the tetrahedral site occupied by $Al^{IV}/(IV)_T$. Data derived from laboratory experiments and analyses reported in Hauri et al. (2006a). Note both orthopyroxenes and clinopyroxenes are included in the regression. Gray line and shaded field are original regression and error envelope from Hauri et al. (2006a; their Fig. 2E). Solid line is the new regression (see discussion), dotted lines represent the calculated error envelope.

Data Repository and Supplemental Information

1. SIMS CALIBRATION OF H_2O IN CLINOPYROXENE

Data for this study were acquired by SIMS over several analytical sessions using the Cameca 6f ion microprobe at the Carnegie Institution of Washington's Department of Terrestrial Magnetism, from 2006 to 2007. The $^{16}O^{1}H/^{30}Si$ signals in the clinopyroxenes were calibrated in reference to the following pyroxene "standards" and their independently-determined H_2O concentrations as given in parentheses (ppm) from Bell et al (1995) and Bell et al (2004): PMR-53 (268), KBH-1-opx (217), ROM271#10 (195), ROM271#16 (439) and ROM271#21 (490). In some sessions, calibration factors were determined directly from linear regression on pyroxene standards, yielding factors that varied from 0.48 – 0.43 (H_2O (wt%)/[$^{16}O^{1}H/^{30}Si$]), as illustrated in Fig. 1b. Calibration involved simple multiplication of $^{16}O^{1}H/^{30}Si$ signals by these factors, without correction of Si explicitly (as in Hauri et al., 2006a and b). The scatter about the lines in Fig. 1b reflects uncertainty in the published H_2O contents of the pyroxene standards, and is not due to matrix effects within the pyroxene compositions (which should only on the order of a few percent, using the method of Hauri et al, 2006b). In other sessions, we used basaltic glass calibrations, which ranged from 0.31 to 0.40 (based on H_2O determinations reported in Hauri 2002; Hauri et al., 2006a and b), and then applied a correction of 1.3846 to account for the off-set in calibration factors between cpx/glass as determined in all sessions from 2006-2007. The off-set is presumably the manifestation of matrix effects between basaltic glass and cpx, possibly similar in cause to those that affect H isotopic fractionation (Hauri et al., 2006b). Fig. 1a shows an example of the glass

calibrations, which are in general better determined than the cpx calibration, but also based on H_2O concentrations well above the range measured in cpx.

2. PARTITIONING OF WATER BETWEEN CPX AND MAFIC MELT

A number of studies have recognized the importance of pyroxene composition, specifically Al, on the crystal/melt partitioning of H_2O (Aubaud et al., 2004; Hauri et al., 2006a; Mierdel et al., 2007; Grant et al., 2007). For example, Hauri et al (2006a) show a positive correlation between $D_{H2O}^{px/liq}$ and the fraction of the tetrahedral site occupied by Al ($Al^{IV}/[IV]_{Total}$), and the expression developed therein is the basis for the calculations in this paper. We have modified the expression, however, to improve upon two related issues. One is that the original regression had the unfortunate result of predicting negative D at zero Al. Second, because of the lack of data for low Al pyroxenes, the errors on the regression became unacceptably large at low $Al^{IV}/[IV]_{Total}$ (and D), causing the calculated H_2O contents of liquid to have very high and uncertain values (because D is in the denominator of the calculation). In order to improve constraints near the origin of the regression of D on $Al^{IV}/[IV]_{Total}$, we have modified it by estimating the D for Al-free pyroxenes using the solubility data of Bromily et al. (2004) for cpx and Rauch and Keppler (2002) for opx, coupled with a model for H_2O solubility in a basaltic melt (Dixon et al., 1995) calculated from 0.3-10 kb. This gives a $D_{H2O}^{px/liq}$ for Al-free pyroxene of 0.001 +/- 0.0005 (where the uncertainty derives from the range in pressure). The y-intercept of the regression is then forced near this point by strongly weighting it in the regression, leading to a slightly different partitioning relationship: $D_{H2O}^{px/liq}$ =

$0.29(Al^{IV}/[IV]_{Total}) + 0.00099$, with uncertainties on the slope and intercept as given in Figure 2. This has the effect of reducing errors in D's calculated when $Al^{IV}/[IV]_{Total} < 0.04$, and of predicting a finite D at zero Al, both of which mark improvements. Clearly further experimental data are welcome in constraining the $D_{H2O}^{cpx/liq}$ for conditions relevant to erupting mafic magmas, but the general coherence in this study between H_2O measured in melt inclusions, and that calculated from cpx, supports a partitioning relationship similar to the one used here.

The use of $Al^{IV}/[IV]_{Total}$ as a pyroxene component follows directly from that published in Hauri et al (2006a), in their Figure 2. In calculating $Al^{IV}/[IV]_{Total}$, pyroxene analyses were first converted from weight percent to single cation fractions, assuming all Fe as Fe^{2+}. The sum of cations on the tetrahedral site include all of the Si, and the sum of the Al^{IV} in the Ca-Tschermak component (CaTs: $CaAl_2SiO_6$), the Cr-Tschermak component (CrTs: $CaCrAlSiO_6$) and Ti-Tschermak component (TiTs: $CaTiAl_2O_6$). The Al^{IV} in each of these components was calculated as follows:

$CrTs^{IV}$ = Cr fraction

$TiTs^{IV}$ = twice the Ti fraction

$CaTs^{IV}$ = 0.5*(Al-[Na+Cr+2Ti]), or the excess Al after assignment to jadeite ($NaAlSi_2O_6$), CrTs and TiTs.

$Al^{IV}/[IV]_{Total}$ is then equal to:

$(CaTs^{IV} + CrTs^{IV} + TiTs^{IV}) / (Si^{IV} + CaTs^{IV} + CrTs^{IV} + TiTs^{IV})$

3. ERRORS IN MAGMATIC WATER ESTIMATES CALCULATED FROM CLINOPYROXENE MEASUREMENTS

There are many sources of error in calculating magmatic water concentrations (C_{H2O}^{liq}) from water measured in clinopyroxene (C_{H2O}^{cpx}), which include the combined uncertainties in (a) the SIMS measurements of H_2O within an analytical session, (b) the calibrations between sessions, (c) the Al^{IV} measurements, and (d) the partitioning relationship outlined above. Here we assess the likely magnitude of these uncertainties, and how they may bear on C_{H2O}^{liq}.

Analytical errors (a) and (c) are the smallest, and can be assessed from multiple analyses collected within nominally homogeneous grains, such as the one shown in Figure 1 (main paper). For example the uncertainty on the measurements at spots h and i within the core of A03-02-cpx16 is < 1% relative for both C_{H2O}^{cpx} and Al^{IV} (Table 1), and so within-run analytical precision can be excellent. Based on replicate analyses over several years of analysis, we take 10% as a conservative estimate of the internal precision. External precision of the H_2O measurements (b), however, approaches 15% relative (2-sigma), based on nearby spots analyzed in different SIMS sessions, reflecting the uncertainties in the different session calibrations (as in Fig 1b of the DR). The calibration slopes in Fig. 1b are indeed reproducible at the 10-15% level, as indicated in the small range in slopes determined over many sessions (0.43 - 0.48), even though the 2-sigma uncertainty on the slope is large (~ 33%) for any given analytical session. This large uncertainty in the absolute value of the slope reflects the scatter of points about the calibration line (Fig 1b), which as discussed above, likely reflects uncertainty in the

published data on the standards derived from different labs by different techniques. We thus consider the precision of the measurements, all made at CIW, to be 15%, but accuracy of the measurements with respect to the range reported by different labs to be 33%.

The total error on C_{H2O}^{liq} also includes (d) the uncertainty on $D^{cpx/liq}$, and as discussed in the prior section, this is difficult to assess. While we have tried to improve the errors that result from the $D_{H2O}^{cpx/liq}$ -Al^{iv} regression (Fig. 2), we do not recommend using the partitioning relationship in Fig 2 (herein) for pyroxenes with $Al^{IV}/[IV]_{Total} < 0.02$, for which there are no experimental data from pyroxene-melt pairs. Such low-Al pyroxenes are not uncommon among evolved, low-pressure arc phenocryst populations. For example, IZ03-17a-cpx2c predicts anomalously high C_{H2O}^{liq} (> 4 wt%) due to a likely spurious low $D_{H2O}^{cpx/liq}$ (0.0046). It is certainly possible that at such low Al contents other substitution mechanisms (e.g., Fe^{3+}) may affect $D_{H2O}^{cpx/liq}$, but these have yet to be determined in such pyroxene compositions. Thus, we recommend using the $D_{H2O}^{cpx/liq}$ expression here, with its error envelope, only for pyroxenes with $Al^{IV}/[IV]_{Total} > 0.02$. The error envelope is derived from a standard York regression, as in Hauri et al (2006a), but the uncertainty is somewhat better than the original due to the Y-intercept constraints discussed above. As shown in Fig. 2, the error on the regression leads to an uncertainty of approximately 10% on $D_{H2O}^{cpx/liq}$.

Propagating all uncertainties into C_{H2O}^{liq} leads to a total error of 35% (2-sigma), which is dominated by the uncertainty in the accuracy of the concentration measurements. For the purposes of comparing relative variations in the data (Figs. 1, 2 and 4 in the main

text), we plot error bars of 17%, which reflect the 2-sigma uncertainty in the external precision and in D, recognizing that the additional uncertainty in the accuracy affects all the data equally (including the melt inclusion data, since these were measured in the same lab as the D's and the cpx, with internally consistent calibration strategies). There is no doubt that future improvements in the SIMS calibrations, in the determination of D, and in the interlaboratory biases, may lead to total uncertainties that approach the precision of the measurements. Nonetheless, even at this time, the method shows promise in the ~ 15% agreement between the cpx population means and those derived independently from melt inclusion data (Fig 3, main text). This provides evidence that the large errors currently associated with the cpx calibrations are not systematic, and lead to accurate population means relative to melt inclusion data collected in the same laboratory.

4. REFERENCES

Aubaud, C., Hauri, E.H., Hirschmann, M., 2004, Hydrogen partition coefficients between nominally anhydrous minerals and basaltic melts: Geophysical Research Letters, v. 31, doi:10.1029/2004GL021341.

Bell D.R., Ihinger, P.D., Rossman, G.R., 1995, Quantitative analysis of hydroxyl in garnet and pyroxene: American Mineralogist, v. 80, p. 465-474.

Bell, D.R., Rossman, G.R., Moore, R.O., 2004, Abundance and partitioning of OH in a high-pressure magmatic system: megacrysts from the Monastery kimberlite, South Africa: Journal of Petrology, v. 45, p. 1-26.

Bromily, G.D., Keppler, H., McCammon, C., Bromily, F.A., Jacobsen,S.D., 2004, Hydrogen solubility and speciation in natural gem-quality chromian diopside: American Mineralogist, v. 89, p. 941-949.

Dixon, J.E., Stolper, E.M., Holloway, J.R., 1995, An experimental study of water and carbon dioxide solubilities in mid-ocean ridge basaltic liquids: Part 1. Calibration and solubility models: Journal of Petrology, v. 36, p. 1607-1631.

Grant, K.J., Kohn, S.C., Brooker, R.A. 2007, The partitioning of water between olivine, orthopyroxene and melt synthesised in the system albite-forsterite-H_2O: Earth and Planetary Science Letter, v. 260, p. 227-241.

Hauri, E.H., Wang,J., Dixon, J.E., King, P.L., Mandeville, C., Newman, S., 2002, SIMS analysis of volatiles in silicate glasses 1. Calibration, matrix effects and comparisons with FTIR: Chemical Geology, v. 183, p. 99-114.

Hauri, E.H., Gaetani, G.A., Green, T.H., 2006a, Partitioning of water during melting of the Earth's upper mantle at H2O-undersaturated conditions: Earth and Planetary Science Letters, v. 248, p. 715-734.

Hauri, E.H., Shaw, A.M., Wang, J., Dixon, J., King, P.L., Mandeville, C., 2006b, Matrix effects in hydrogen isotope analysis of silicate glasses by SIMS: Chemical Geology, v. 235, no. 3-4, p. 352-365.

Mierdel, K., Keppler, H., Smyth, J.R., Langenhorst, F., 2007, Water Solubility in Aluminous Orthopyroxene and the Origin of Earth's Asthenosphere: Science, v. 315, no. 5810, p. 364 – 368.

Rauch, M., Keppler, H., 2002, Water solubility in orthopyroxene: Contributions to Mineralogy and Petrology, v. 143, p. 525-536.

Sample	cpx#	(μm x μm)	pt	μm from rim	H_2O (ppm)	H_2O_{cpx} error (ppm)	Al^{IV}/total(IV)	D_{H2O}	H_2O_{liq} (wt%)	H_2O_{liq} error
AR03-02	2	775 x >550	a	60	810	122	0.064	0.0194	4.17	0.7082
AR03-02	2	775 x >550	c	105	869	130	0.063	0.0193	4.51	0.7661
AR03-02	2	775 x >550	b	355	850	128	0.059	0.0181	4.71	0.8002
AR03-02	5	>815 x 625	a	40	780	117	0.058	0.0178	4.37	0.7430
AR03-02	5	>815 x 625	e	50	944	142	0.070	0.0214	4.41	0.7501
AR03-02	5	>815 x 625	b	230	823	123	0.070	0.0214	3.84	0.6534
AR03-02	5	>815 x 625	d	270	974	146	0.070	0.0212	4.60	0.7815
AR03-02	5	>815 x 625	c	480	909	136	0.070	0.0214	4.25	0.7225
AR03-02	6	1130 x >610	d	65	293	44	0.048	0.0148	1.97	0.3354
AR03-02	6	1130 x >610	a	110	544	82	0.032	0.0102	5.32	0.9050
AR03-02	6	1130 x >610	c	460	530	80	0.031	0.0099	5.35	0.9098
AR03-02	6	1130 x >610	b	500	546	82	0.032	0.0103	5.29	0.8995

Data Repository Table DR1

AR03-02 is scoria lapilli from Arenal volcano, Costa Rica (Wade et al., 2006)

IZ03-17a is scoria lapilli from Irazu volcano, Costa Rica (Benjamin et al., 2007)

GL-G2 is basaltic bomb from Galunggung volcano, Java (Kelley et al., in prep)

05AUNY17 is basaltic hyaloclastite from Augustine volcano, AK (Zimmer et al., in prep)

Rims were confirmed in most grains from adhered glass at the grain edge, and in these cases the transect ran from the rim towards the core.

Some cores were confirmed by whole-grain compositional mapping by EMP.

If a grain was broken, the minimum crystal length and distance to the closest rim are reported.

H2O (ppm) in cpx measured by SIMS ion microprobe at the Carnegie Institution of Washington (methods in text that accompany this table)

Al (IV)/(IV)total is the molar fraction of the tetrahedra site occupied by Al. Calculated as given in the text that accompanies this table

D(H2O) is cpx/liq partition coefficient, calculated from: D = (Al in IV)*0.29 + 0.00099, after Hauri et al (2006a),
modified as described in the text that accompanies this table

Error on H2O concentration in cpx is 15%, based on external precision of the SIMS measurements.
Uncertainty on the accuracy approaches 33%, given the scatter in the cpx calibration shown in Fig 1b, due to interlaboratory differences.

H2O-liq calculated from: H2O(cpx)/D

Major element analyses by electron microprobe at MIT; in spots adjacent to SIMS analyses

Mg# is molar ratio of Mg to (Mg+FeT) in cpx

Error on C(H2O)liq calculated by propagating errors in the numerator (+/-15% on the H2O measurements) and in the denominator
(from the ~ 10% error on D error given by the error on the regression in Fig. 2).

Wade DR1b

Sample	SiO2 (wt%)	TiO2 (wt%)	Al2O3 (wt%)	FeO (wt%)	MnO (wt%)	MgO (wt%)	CaO (wt%)	Na2O (wt%)	Cr (ppm)	Total	Mg# (molar)
AR03-02	49.90	0.40	5.65	8.39	0.18	13.98	21.45	0.27	287	100.26	74.8
AR03-02	50.26	0.39	5.70	8.48	0.24	13.85	21.47	0.28	72	100.69	74.4
AR03-02	50.69	0.44	5.34	8.44	0.22	14.33	21.04	0.33	142	100.85	75.2
AR03-02	50.66	0.63	4.87	6.39	0.14	14.83	22.98	0.30	1263	100.99	80.5
AR03-02	50.17	0.49	6.21	6.28	0.14	14.82	21.70	0.32	1390	100.32	80.8
AR03-02	50.27	0.52	6.22	6.40	0.22	14.76	21.92	0.34	1372	100.87	80.4
AR03-02	50.55	0.53	6.13	6.16	0.17	15.10	22.35	0.30	1192	101.46	81.4
AR03-02	50.43	0.51	6.22	6.20	0.15	14.79	22.18	0.33	1494	101.02	81.0
AR03-02	50.32	0.53	4.26	9.50	0.27	14.43	20.31	0.41		100.03	73.0
AR03-02	51.85	0.38	2.98	8.66	0.27	15.29	20.76	0.35		100.53	75.9
AR03-02	51.79	0.36	2.95	9.39	0.36	15.70	20.40	0.39		101.34	74.9
AR03-02	52.38	0.41	2.97	8.82	0.26	15.23	20.98	0.34		101.39	75.5

Data Repository Table DR1

AR03-02 is scoria lapilli from Arenal volcano, Costa Rica (Wade et al., 2006)

IZ03-17a is scoria lapilli from Irazu volcano, Costa Rica (Benjamin et al., 2007)

GL-G2 is basaltic bomb from Galunggung volcano, Java (Kelley et al., in prep)

05AUNY17 is basaltic hyaloclastite from Augustine volcano, AK (Zimmer et al., in prep)

Rims were confirmed in most grains from adhered glass at the grain edge, and in these cases the transect ran from the rim towards the core.

Some cores were confirmed by whole-grain compositional mapping by EMP.

If a grain was broken, the minimum crystal length and distance to the closest rim are reported.

H2O (ppm) in cpx measured by SIMS ion microprobe at the Carnegie Institution of Washington (methods in text that accompany this table)

Al (IV)/(IV)total is the molar fraction of the tetrahedra site occupied by Al. Calculated as given in the text that accompanies this table

D(H2O) is cpx/liq partition coefficient, calculated from: D = (Al in IV)*0.29 + 0.00099, after Hauri et al (2006a), modified as described in the text that accompanies this table

Error on H2O concentration in cpx is 15%, based on external precision of the SIMS measurements. Uncertainty on the accuracy approaches 33%, given the scatter in the cpx calibration shown in Fig 1b, due to interlaboratory differences.

H2O-liq calculated from: H2O(cpx)/D

Major element analyses by electron microprobe at MIT; in spots adjacent to SIMS analyses

Mg# is molar ratio of Mg to (Mg+FeT) in cpx

Error on C(H2O)liq calculated by propagating errors in the numerator (+/-15% on the H2O measurements) and in the denominator (from the ~ 10% error on D error given by the error on the regression in Fig. 2).

Wade DR1c

Sample	cpx#	(μm x μm)	pt	μm from rim	H_2O (ppm)	H_2O_{cpx} error	Al^{IV}/total(IV)	D_{H2O}	H_2O_{liq} (wt%)	H_2O_{liq} error
AR03-02	9	1000 x 500	a	50	271	41	0.056	0.0171	1.58	0.2690
AR03-02	9	1000 x 500	d	60	295	44	0.036	0.0115	2.56	0.4356
AR03-02	9	1000 x 500	e	65	204	31	0.037	0.0116	1.76	0.2992
AR03-02	9	1000 x 500	b	180	181	27	0.017	0.0060	3.00	0.5104
AR03-02	15	1100 x 740	d	50	879	132	0.072	0.0218	4.03	0.6859
AR03-02	15	1100 x 740	e	60	731	110	0.077	0.0232	3.15	0.5356
AR03-02	15	1100 x 740	c	130	1175	176	0.070	0.0213	5.53	0.9399
AR03-02	15	1100 x 740	b	300	1013	152	0.071	0.0217	4.67	0.7937
AR03-02	16	>610 x 550	a	50	199	30	0.027	0.0089	2.25	0.3821
AR03-02	16	>610 x 550	k	50	231	35	0.031	0.0100	2.31	0.3927
AR03-02	16	>610 x 550	b	90	429	64	0.042	0.0131	3.28	0.5581
AR03-02	16	>610 x 550	j	90	409	61	0.043	0.0135	3.03	0.5155
AR03-02	16	>610 x 550	c	125	608	91	0.048	0.0150	4.06	0.6894
AR03-02	16	>610 x 550	i	135	627	94	0.052	0.0161	3.89	0.6619
AR03-02	16	>610 x 550	h	170	627	94	0.052	0.0160	3.92	0.6657
AR03-02	16	>610 x 550	d	175	613	92	0.050	0.0155	3.95	0.6710
AR03-02	16	>610 x 550	g	210	518	78	0.049	0.0151	3.43	0.5823
AR03-02	16	>610 x 550	e	225	584	88	0.047	0.0146	4.00	0.6796
AR03-02	16	>610 x 550	f	280	537	81	0.049	0.0152	3.52	0.5991
AR03-02	17	>1300 x 720	a	60	992	149	0.071	0.0217	4.57	0.7763
AR03-02	17	>1300 x 720	c	65	1057	159	0.075	0.0226	4.68	0.7951
AR03-02	17	>1300 x 720	b	390	1062	159	0.078	0.0237	4.48	0.7620
AR03-02	18	500 x 400	a	50	256	38	0.033	0.0106	2.41	0.4093
AR03-02	18	500 x 400	b	70	555	83	0.040	0.0127	4.36	0.7412
AR03-02	18	500 x 400	c	240	780	117	0.061	0.0188	4.16	0.7066
AR03-02	19	1000 x 620	a	50	792	119	0.068	0.0207	3.83	0.6516
AR03-02	19	1000 x 620	e	80	679	102	0.042	0.0131	5.18	0.8803
AR03-02	19	1000 x 620	b	200	933	140	0.066	0.0200	4.66	0.7914
AR03-02	19	1000 x 620	d	250	532	80	0.066	0.0201	2.65	0.4506
AR03-02	19	1000 x 620	c	370	874	131	0.069	0.0211	4.14	0.7046
AR03-02	20	710 x >400	b	300	553	83	0.056	0.0172	3.22	0.5474

Wade DR1d

Sample	SiO2 (wt%)	TiO2 (wt%)	Al2O3 (wt%)	FeO (wt%)	MnO (wt%)	MgO (wt%)	CaO (wt%)	Na2O (wt%)	Cr (ppm)	Total	Mg# (molar)
AR03-02	51.56	0.93	4.43	6.55	0.16	15.23	22.20	0.35	1141	101.58	80.6
AR03-02	52.58	0.65	3.00	6.19	0.19	14.34	22.51	0.33	779	99.91	80.5
AR03-02	52.56	0.62	2.99	6.04	0.17	15.12	22.07	0.29	809	99.98	81.7
AR03-02	53.45	0.62	1.48	9.13	0.31	15.00	20.92	0.41	65	101.33	74.5
AR03-02	50.11	0.55	6.16	6.79	0.14	14.98	22.19	0.32	935	101.38	79.7
AR03-02	49.07	0.47	6.82	8.20	0.20	13.68	21.99	0.32	130	100.78	74.8
AR03-02	49.83	0.51	6.30	7.65	0.23	14.24	21.88	0.34	1162	101.14	76.8
AR03-02	50.22	0.50	6.26	8.75	0.26	14.19	22.14	0.31	57	102.64	74.3
AR03-02	52.69	0.46	2.33	8.90	0.25	16.00	20.99	0.26	0	101.89	76.2
AR03-02	52.34	0.50	2.56	9.13	0.28	15.53	20.53	0.22		101.08	75.2
AR03-02	52.67	0.26	3.78	6.11	0.15	16.93	21.44	0.24	1767	101.84	83.2
AR03-02	52.65	0.26	3.81	6.02	0.10	16.77	21.63	0.19	2029	101.74	83.2
AR03-02	51.38	0.26	4.54	5.78	0.08	16.24	21.86	0.37	1554	100.74	83.4
AR03-02	51.94	0.26	4.81	6.00	0.08	16.21	21.95	0.28	1798	101.80	82.8
AR03-02	52.03	0.24	4.91	6.01	0.04	16.26	21.77	0.34	1621	101.84	82.8
AR03-02	52.28	0.28	4.69	6.08	0.08	16.34	21.82	0.31	1398	102.08	82.7
AR03-02	52.01	0.29	4.54	5.92	0.11	16.34	21.86	0.32	1524	101.60	83.1
AR03-02	52.26	0.23	4.45	6.03	0.13	16.45	21.97	0.32	1498	102.07	83.0
AR03-02	52.16	0.27	4.53	5.80	0.13	16.29	22.12	0.27	1419	101.77	83.4
AR03-02	50.36	0.48	6.55	7.62	0.20	13.89	21.88	0.37	314	101.40	76.5
AR03-02	49.51	0.46	6.79	7.48	0.13	14.07	21.85	0.39	283	100.72	77.0
AR03-02	49.19	0.56	6.93	7.82	0.15	14.14	21.85	0.35	268	101.02	76.3
AR03-02	51.86	0.41	3.10	9.29	0.27	15.02	20.49	0.37	140	100.83	74.2
AR03-02	51.58	0.52	3.49	9.23	0.29	14.83	20.85	0.28	83	101.08	74.1
AR03-02	50.33	0.51	5.47	8.91	0.30	14.25	21.08	0.34	237	101.23	74.0
AR03-02	50.16	0.43	6.18	7.45	0.15	14.33	21.61	0.34	164	100.67	77.4
AR03-02	51.58	0.48	3.77	9.58	0.30	14.72	20.44	0.35	163	101.24	73.3
AR03-02	50.57	0.51	5.88	7.17	0.22	14.64	21.92	0.32	261	101.28	78.4
AR03-02	50.87	0.52	5.87	7.47	0.21	14.41	22.28	0.29	225	101.96	77.5
AR03-02	50.62	0.51	6.15	7.19	0.17	14.86	21.60	0.26	294	101.40	78.7
AR03-02	51.59	0.39	4.82	5.87	0.14	15.12	22.00	0.27	3079	100.66	82.1

Wade DR1e

Sample	cpx#	(μm x μm)	pt	μm from rim	H_2O (ppm)	H_2O_{cpx} error (ppm)	Al^{IV}/total(IV)	D_{H2O}	H_2O_{liq} (wt%)	H_2O_{liq} error
IZ03-17a	2	750 x 410	a	50	273	41	0.036	0.0115	2.38	0.4049
IZ03-17a	2	750 x 410	b	110	321	48	0.050	0.0155	2.07	0.3521
IZ03-17a	2	750 x 410	c	230	223	33	0.012	0.0046	4.85	0.8239
IZ03-17a	2	750 x 410	d	>110	194	29	0.015	0.0053	3.64	0.6186
IZ03-17a	8	500 x 240	a	120	282	42	0.053	0.0163	1.73	0.2942
IZ03-17a	16	1000 x 500	c	50	205	31	0.051	0.0158	1.30	0.2213
IZ03-17a	16	1000 x 500	a	60	275	41	0.031	0.0100	2.76	0.4696
IZ03-17a	16	1000 x 500	b	250	258	39	0.031	0.0099	2.62	0.4450
IZ03-17a	17	500 x 500	a	110	196	29	0.027	0.0090	2.19	0.3721
IZ03-17a	17	500 x 500	c	110	150	23	0.019	0.0066	2.27	0.3852
IZ03-17a	17	500 x 500	b	250	187	28	0.018	0.0063	2.99	0.5079
IZ03-17a	22	>1000 x >300	b	170	432	65	0.042	0.0131	3.31	0.5624
IZ03-17a	23	>1000 x >900	a	80	485	73	0.052	0.0161	3.01	0.5123
IZ03-17a	23	>1000 x >900	b	250	404	61	0.032	0.0102	3.95	0.6717
IZ03-17a	23	>1000 x >900	c	375	363	54	0.035	0.0112	3.24	0.5514
IZ03-17a	28	>1060 x >500	a	50	373	56	0.065	0.0199	1.87	0.3179
IZ03-17a	28	>1060 x >500	d	125	457	69	0.050	0.0155	2.95	0.5010
IZ03-17a	28	>1060 x >500	b	180	492	74	0.054	0.0166	2.96	0.5029
IZ03-17a	28	>1060 x >500	c	270	502	75	0.057	0.0175	2.87	0.4871
GL-G2	1	>700 x >500	c	>200	97	14	0.062	0.0191	0.51	0.0861
GL-G2	3	>1000 x >750	g	60	53	8	0.064	0.0195	0.27	0.0459
GL-G2	3	>1000 x >750	f	250	87	13	0.057	0.0175	0.50	0.0848
GL-G2	4	>750 x >550	d	130	73	11	0.050	0.0154	0.47	0.0807
GL-G2	4	>750 x >550	e	>180	75	11	0.048	0.0148	0.51	0.0859
GL-G2	5	>1300 x >250	d	>60	64	10	0.052	0.0160	0.40	0.0681
GL-G2	6	>800 x >500	f	100	119	18	0.076	0.0231	0.52	0.0877
GL-G2	6	>800 x >500	g	250	117	18	0.095	0.0284	0.41	0.0699

Wade DR1f

Sample	SiO2 (wt%)	TiO2 (wt%)	Al2O3 (wt%)	FeO (wt%)	MnO (wt%)	MgO (wt%)	CaO (wt%)	Na2O (wt%)	Cr (ppm)	Total	Mg# (molar)
IZ03-17a	52.28	0.95	2.67	7.91	0.21	15.93	21.58	0.36	274	101.92	78.2
IZ03-17a	50.82	0.80	3.98	6.50	0.15	15.52	22.90	0.34	1018	101.17	81.0
IZ03-17a	53.12	0.46	1.41	8.63	0.38	14.98	21.24	0.54	205	100.80	75.6
IZ03-17a	52.83	0.49	1.43	8.34	0.34	15.21	21.23	0.43	194	100.32	76.5
IZ03-17a	50.93	0.86	4.06	6.43	0.15	15.06	22.85	0.29	1350	100.82	80.7
IZ03-17a	51.53	0.75	4.07	6.13	0.18	15.24	22.84	0.27	1193	101.17	81.6
IZ03-17a	53.23	0.53	2.49	5.84	0.14	16.12	22.22	0.25	1366	101.03	83.1
IZ03-17a	53.45	0.52	2.53	5.65	0.18	16.46	22.91	0.26	1035	102.11	83.9
IZ03-17a	52.69	0.87	2.19	9.84	0.44	14.40	20.30	0.49	327	101.28	72.3
IZ03-17a	52.74	0.56	1.67	8.74	0.42	15.22	20.70	0.39	256	100.47	75.6
IZ03-17a	53.17	0.60	1.66	9.53	0.36	15.08	20.78	0.48	315	101.71	73.8
IZ03-17a	52.19	0.65	3.53	8.23	0.23	15.03	21.58	0.32	174	101.80	76.5
IZ03-17a	51.71	0.60	3.84	4.68	0.10	15.89	23.18	0.26	6523	101.23	85.8
IZ03-17a	53.62	0.42	2.41	3.96	0.10	16.27	23.48	0.22	4144	101.09	88.0
IZ03-17a	53.48	0.59	2.86	5.63	0.16	16.26	22.41	0.25	1096	101.82	83.7
IZ03-17a	50.74	0.94	5.04	5.78	0.10	14.98	22.97	0.31	2904	101.29	82.2
IZ03-17a	51.82	0.58	3.65	4.33	0.09	15.40	23.64	0.25	6739	100.75	86.4
IZ03-17a	51.11	0.80	4.25	6.09	0.11	15.06	23.04	0.32	2044	101.08	81.5
IZ03-17a	50.95	0.69	4.19	5.06	0.10	15.30	23.62	0.19	4846	100.81	84.3
GL-G2	51.31	0.70	5.07	5.02	0.11	14.85	23.65	0.26	2525	101.35	84.1
GL-G2	50.53	0.87	4.43	7.85	0.19	14.53	22.08	0.32	1701	101.04	76.7
GL-G2	49.96	0.75	4.81	6.33	0.13	13.67	22.60	0.30	4930	99.28	79.4
GL-G2	51.91	0.50	4.25	5.13	0.15	15.17	23.39	0.28	1762	101.04	84.1
GL-G2	51.61	0.48	4.01	5.65	0.15	15.52	23.24	0.23	1452	101.09	83.0
GL-G2	51.28	0.59	4.29	7.79	0.23	14.33	22.56	0.23	759	101.41	76.6
GL-G2	50.20	0.78	5.97	5.28	0.15	14.35	23.49	0.22	4288	101.07	82.9
GL-G2	48.83	1.11	7.17	6.22	0.14	13.60	23.34	0.21	4430	101.27	79.6

Sample	cpx#	(μm x μm)	pt	μm from rim	H_2O (ppm)	H_2O_{cpx} error (ppm)	Al^{IV}/total(IV)	D_{H2O}	H_2O_{liq} (wt%)	H_2O_{liq} error
05AUNY17	1	1050 x 950	a	25	680	102	0.042	0.0132	5.16	0.8773
05AUNY17	1	1050 x 950	f	110	555	83	0.055	0.0168	3.30	0.5602
05AUNY17	1	1050 x 950	b	200	584	88	0.041	0.0129	4.53	0.7707
05AUNY17	1	1050 x 950	e	280	606	91	0.035	0.0112	5.42	0.9206
05AUNY17	1	1050 x 950	c	410	566	85	0.042	0.0132	4.28	0.7273
05AUNY17	1	1050 x 950	d	420	561	84	0.043	0.0134	4.18	0.7108
05AUNY17	2	1200 x 685	a	90	283	42	0.022	0.0075	3.79	0.6444
05AUNY17	2	1200 x 685	b	270	326	49	0.022	0.0073	4.44	0.7552
05AUNY17	2	1200 x 685	f	280	342	51	0.022	0.0073	4.66	0.7923
05AUNY17	2	1200 x 685	e	465	449	67	0.020	0.0069	6.48	1.1011
05AUNY17	2	1200 x 685	d	600	367	55	0.024	0.0080	4.57	0.7777
05AUNY17	3	1270 x 1100	g	125	702	105	0.046	0.0144	4.88	0.8302
05AUNY17	3	1270 x 1100	f	300	626	94	0.031	0.0100	6.28	1.0684
05AUNY17	3	1270 x 1100	c	400	548	82	0.033	0.0105	5.23	0.8893
05AUNY17	3	1270 x 1100	e	500	560	84	0.063	0.0193	2.90	0.4929
05AUNY17	3	1270 x 1100	d	625	510	77	0.043	0.0133	3.82	0.6497
05AUNY17	4	880 x 610	a	60	486	73	0.054	0.0166	2.92	0.4968
05AUNY17	4	880 x 610	e	80	629	94	0.040	0.0126	4.99	0.8490
05AUNY17	4	880 x 610	d	200	717	108	0.048	0.0149	4.83	0.8213
05AUNY17	4	880 x 610	b	210	642	96	0.064	0.0195	3.30	0.5603
05AUNY17	4	880 x 610	c	325	649	97	0.062	0.0188	3.45	0.5862
05AUNY17	5	1000 x 500	a	160	783	117	0.063	0.0191	4.09	0.6954
05AUNY17	5	1000 x 500	c	200	595	89	0.047	0.0145	4.11	0.6980
05AUNY17	5	1000 x 500	b	480	727	109	0.053	0.0164	4.44	0.7544
05AUNY17	6	1170 x 800	f	90	330	49	0.031	0.0101	3.26	0.5544
05AUNY17	6	1170 x 800	e	225	243	37	0.021	0.0072	3.39	0.5769
05AUNY17	6	1170 x 800	b	300	522	78	0.038	0.0119	4.40	0.7477
05AUNY17	6	1170 x 800	c	480	437	66	0.023	0.0076	5.76	0.9787
05AUNY17	6	1170 x 800	d	500	384	58	0.021	0.0070	5.52	0.9387

Wade DR1h

Sample	SiO2 (wt%)	TiO2 (wt%)	Al2O3 (wt%)	FeO (wt%)	MnO (wt%)	MgO (wt%)	CaO (wt%)	Na2O (wt%)	Cr (ppm)	Total	Mg# (molar)
05AUNY17	51.48	0.44	3.61	6.19	0.05	15.37	22.42	0.24	522	99.81	81.2
05AUNY17	50.47	0.55	4.55	6.75	0.05	15.12	22.45	0.20	265	100.14	79.6
05AUNY17	51.51	0.42	3.57	6.55	0.07	15.62	22.49	0.24	271	100.47	80.6
05AUNY17	51.59	0.30	3.11	6.69	0.10	15.39	21.35	0.22	536	98.75	80.0
05AUNY17	51.27	0.45	3.59	6.46	0.08	15.72	21.96	0.22	353	99.76	80.9
05AUNY17	51.32	0.42	3.64	6.66	0.10	15.60	22.03	0.18	176	99.95	80.3
05AUNY17	53.53	0.17	1.87	4.65	0.04	17.98	21.89	0.23	3912	100.35	87.1
05AUNY17	53.64	0.13	1.81	4.29	0.04	17.51	21.55	0.17	3486	99.13	87.7
05AUNY17	53.56	0.15	1.84	4.12	0.05	17.83	21.81	0.19	3128	99.56	88.3
05AUNY17	53.56	0.16	1.71	4.37	0.03	18.12	21.70	0.18	2898	99.83	87.8
05AUNY17	53.27	0.14	2.00	4.19	0.02	17.90	22.00	0.19	4026	99.70	88.1
05AUNY17	52.16	0.31	2.67	5.77	0.06	16.58	21.87	0.21	1065	99.63	83.3
05AUNY17	49.57	0.62	5.28	6.79	0.03	14.71	22.52	0.28	538	99.80	79.0
05AUNY17	52.34	0.36	2.79	5.87	0.08	16.46	22.25	0.18	609	100.33	83.0
05AUNY17	50.94	0.41	3.89	6.39	0.04	15.51	22.65	0.17	556	100.01	80.8
05AUNY17	52.16	0.31	2.67	5.77	0.06	16.58	21.87	0.21	1065	99.63	83.3
05AUNY17	50.65	0.75	4.32	7.65	0.15	15.09	21.04	0.24	274	99.89	77.4
05AUNY17	51.52	0.38	3.52	6.34	0.09	15.38	21.98	0.24	367	99.46	80.8
05AUNY17	51.17	0.49	4.07	6.61	0.10	15.18	21.64	0.23	326	99.48	80.0
05AUNY17	50.10	0.56	5.42	6.78	0.09	14.45	22.51	0.27	1074	100.19	78.8
05AUNY17	49.67	0.60	5.07	6.87	0.08	14.96	22.25	0.24	910	99.75	79.1
05AUNY17	50.13	0.63	5.21	6.99	0.09	14.55	22.21	0.22	404	100.03	78.4
05AUNY17	50.80	0.43	4.08	6.77	0.08	15.26	21.72	0.27	176	99.41	79.7
05AUNY17	50.48	0.52	4.44	6.80	0.07	15.22	22.31	0.21	483	100.05	79.6
05AUNY17	52.49	0.24	2.74	6.17	0.14	16.71	21.06	0.15	899	99.69	82.5
05AUNY17	53.61	0.18	1.87	4.39	0.05	17.34	22.17	0.16	1404	99.77	87.3
05AUNY17	51.70	0.32	3.12	5.53	0.05	16.39	22.53	0.21	2326	99.84	83.7
05AUNY17	53.62	0.17	1.99	4.15	0.02	17.47	22.41	0.24	2997	100.07	88.0
05AUNY17	53.41	0.17	1.88	4.47	0.03	17.60	22.23	0.19	1306	99.98	87.3